

## A variational method for density functional theory calculations on metallic systems with thousands of atoms

Álvaro Ruiz-Serrano and Chris-Kriton Skylaris

Citation: *J. Chem. Phys.* **139**, 054107 (2013); doi: 10.1063/1.4817001

View online: <http://dx.doi.org/10.1063/1.4817001>

View Table of Contents: <http://jcp.aip.org/resource/1/JCPSA6/v139/i5>

Published by the AIP Publishing LLC.

---

### Additional information on J. Chem. Phys.

Journal Homepage: <http://jcp.aip.org/>

Journal Information: [http://jcp.aip.org/about/about\\_the\\_journal](http://jcp.aip.org/about/about_the_journal)

Top downloads: [http://jcp.aip.org/features/most\\_downloaded](http://jcp.aip.org/features/most_downloaded)

Information for Authors: <http://jcp.aip.org/authors>



**Goodfellow**

metals • ceramics • polymers  
composites • compounds • glasses

**Save 5% • Buy online**  
70,000 products • Fast shipping

# A variational method for density functional theory calculations on metallic systems with thousands of atoms

Álvaro Ruiz-Serrano and Chris-Kriton Skylaris<sup>a)</sup>

*School of Chemistry, University of Southampton, Highfield, Southampton SO17 1BJ, United Kingdom*

(Received 8 May 2013; accepted 16 July 2013; published online 2 August 2013)

A new method for finite-temperature density functional theory calculations which significantly increases the number of atoms that can be simulated in metallic systems is presented. A self-consistent, direct minimization technique is used to obtain the Helmholtz free energy of the electronic system, described in terms of a set of non-orthogonal, localized functions which are optimized *in situ* using a periodic-sinc basis set, equivalent to plane waves. Most parts of the calculation, including the demanding operation of building the Hamiltonian matrix, have a computational cost that scales linearly with the number of atoms in the system. Also, this approach ensures that the Hamiltonian matrix has a minimal size, which reduces the computational overhead due to diagonalization, a cubic-scaling operation that is still required. Large basis set accuracy is retained via the optimization of the localized functions. This method allows accurate simulations of entire metallic nanostructures, demonstrated with calculations on a supercell of bulk copper with 500 atoms and on gold nanoparticles with up to 2057 atoms. © 2013 AIP Publishing LLC. [<http://dx.doi.org/10.1063/1.4817001>]

## I. INTRODUCTION

Kohn-Sham density functional theory (KS-DFT)<sup>1,2</sup> is broadly used for atomistic simulations in the quantum scale to accurately predict the electronic, optical, structural, and other properties of a wide range of molecules and materials. Plane-waves<sup>3</sup> are the natural choice of basis set functions to study crystalline and periodic systems. Programs such as CASTEP,<sup>4</sup> VASP,<sup>5</sup> QUANTUM ESPRESSO,<sup>6</sup> or ABINIT<sup>7</sup> use plane-waves and pseudopotentials for the core electrons, while programs such as GPAW<sup>8</sup> also use plane-waves and the all-electron projector augmented-wave method.<sup>9</sup> Other choices of basis sets, such as Gaussian functions,<sup>10–12</sup> Slater-type orbitals,<sup>13</sup> or numerical orbitals,<sup>14–20</sup> are also available for organic or metallic materials. The cost of traditional KS-DFT scales as  $\mathcal{O}(N^3)$  with the number of atoms in the system,  $N$ , which typically limits the range of systems that can be simulated. Nevertheless, linear-scaling KS-DFT approaches,<sup>21</sup> in which the cost scales as  $\mathcal{O}(N)$ , have been developed for insulators and semiconductors, based on the principle of nearsightedness of the electronic matter.<sup>22,23</sup> Programs such as ONETEP,<sup>24</sup> CONQUEST,<sup>25</sup> SIESTA,<sup>26</sup> OPENMX,<sup>27</sup> or BIGDFT<sup>28</sup> use this approach to perform calculations on tens of thousands of atoms. In spite of this, calculations on metallic systems remain limited by their cubic-scaling behavior, requiring either a small number of atoms or large computational resources. Some examples of recent KS-DFT studies on metallic compounds are nanoparticles for catalytic processes,<sup>29–31</sup> interactions at metallic surfaces,<sup>32–34</sup> and characterization of alloys and amorphous materials.<sup>35–37</sup>

In practise, simulations on metals are more difficult than on insulators or semiconductors. Self-consistent approaches can suffer the phenomenon of level crossing<sup>5</sup> due to the lack

of a band-gap in the vicinity of the Fermi level. Mermin's extension of DFT to finite-temperature statistical ensembles,<sup>38</sup> and the subsequent development of finite-temperature KS-DFT,<sup>39</sup> allowed calculations on metals to be performed efficiently. Within this formalism, the KS states have occupancies determined by a probability distribution regulated by a constant electronic temperature. This nondeterministic view of the occupancies results in an entropy term that must be taken into account. The Helmholtz free energy combines the KS energy and the entropy in a single functional that obeys the variational principle. A process to find the KS ground state by minimizing the free energy self-consistently can now be envisaged, commonly using either density mixing<sup>5,40,41</sup> or direct minimization techniques.<sup>42–45</sup>

In this work, the new method for performing finite-temperature KS-DFT calculations on large metallic systems with the ONETEP program,<sup>24</sup> using a direct free energy minimization technique, is presented. The algorithm follows the two nested loop approach of Marzari *et al.*<sup>44</sup> to minimize the free energy functional with respect to the occupancies in a non-diagonal representation and a set of non-canonical orbitals. However, for the inner loop, the present implementation follows the method of Freysoldt *et al.*<sup>45</sup> based on a line-search in the space of non-diagonal Hamiltonian matrices. Most importantly, the implementation described in this work uses localized non-orthogonal functions optimized *in situ*, instead of non-canonical, delocalized orbitals.<sup>46–50</sup> Within the formalism of ONETEP, the KS orbitals are expanded in terms of a minimal set of non-orthogonal generalized Wannier functions (NGWFs)<sup>51</sup> which are strictly localized within spheres in real space and are variationally optimized in terms of a basis set of periodic-sinc (psinc) functions.<sup>52</sup> The psinc functions are equivalent to a plane-wave basis set, and allow the core electrons to be efficiently described with pseudopotentials.

<sup>a)</sup>Electronic mail: C.Skylaris@soton.ac.uk

The localization constraint ensures that the matrix representation of operators such as the Hamiltonian is sparse, facilitating the use of efficient, highly parallel sparse algebra routines to achieve linear-scaling computational cost on most of the parts of the algorithm.<sup>53</sup> The exception is the diagonalization of the Hamiltonian matrix, which remains cubic-scaling. However, the idea behind this method, following the advances by Fattebert and Bernholc,<sup>50</sup> is that, with the use of strictly localized functions, the dimensions of the Hamiltonian matrix are reduced to the minimum, and as a result, the overhead due to diagonalization of the Hamiltonian is also minimum. The immediate consequence of this approach is that the largest computational effort is shifted towards the parts of the algorithm that are linear-scaling, and chemical accuracy is achieved with the *in situ* optimization of the NGWFs. As the number of atoms in the system increases, the diagonalization step starts to be more expensive, and eventually it will dominate the calculation. Parallel eigensolvers such as those included in the ScaLAPACK package<sup>50,54</sup> have the potential to distribute the computational and memory requirements over a large number of processors. The tests presented in this work show that the crossover point is in the range of a few thousand atoms on a relatively modest number of processors. This is a favourable result that enables calculations on large metallic systems of many thousands of atoms to be achieved, at a computational cost that is significantly reduced with respect to most traditional cubic-scaling KS-DFT approaches.

This work is structured as follows. In Sec. II, the principles of finite temperature KS-DFT are outlined. Then, in Sec. III, the approach based on the expansion of the KS orbitals in terms of NGWFs, and its implementation in the ONETEP program, are described. Section IV offers a detailed description of the algorithm for direct minimization of the Helmholtz free energy functional, which employs two nested loops to find the KS ground-state in an iterative, variational manner. Section V includes the results. First, the performance of the algorithm with increasing number of atoms in the system is studied. Then, the results of validation tests are shown. These include calculations on a small Pt nanoparticle and on periodic bulk Cu with 500 atoms in the simulation cell, for which very good agreement with the results obtained with the CASTEP<sup>4</sup> program is demonstrated. To conclude, a series of calculations on Au cuboctahedral nanoparticles of up to 2057 atoms were successfully completed using the method presented in this work.

## II. FINITE-TEMPERATURE KS-DFT

At the ground state, a system of  $N_e$  interacting electrons satisfies the KS equation

$$\hat{H} |\psi_i\rangle = \epsilon_i |\psi_i\rangle, \quad (1)$$

where  $\{|\psi_i\rangle\}$  are orthonormal KS states,  $\{\epsilon_i\}$  are the energy eigenvalues, and  $\hat{H}$  is the Hamiltonian operator given by

$$\hat{H} = \hat{T} + \hat{V}_{ext} + \hat{V}_H[n] + \hat{V}_{XC}[n]. \quad (2)$$

In this equation,  $\hat{T}$  is the kinetic energy operator,  $\hat{V}_{ext}$  is the external potential operator,  $\hat{V}_H[n]$  is the Hartree operator, and  $\hat{V}_{XC}[n]$  is the exchange-correlation operator, re-

spectively. The last two terms depend explicitly upon the electronic density,  $n(\mathbf{r})$ , defined as

$$n(\mathbf{r}) = \sum_i f_i \psi_i(\mathbf{r}) \psi_i^*(\mathbf{r}), \quad (3)$$

where  $\{f_i\}$  are the occupancies associated to  $\{|\psi_i\rangle\}$ . The values of  $\{f_i\}$  are calculated as a function of  $\{\epsilon_i\}$ , following the *aufbau* principle, according to the Fermi-Dirac distribution

$$f_i(\epsilon_i) = \left(1 + \exp\left[\frac{\epsilon_i - \mu}{k_B T}\right]\right)^{-1}, \quad (4)$$

where  $T$  is a finite electronic temperature,  $\mu$  is the Fermi level, and  $k_B$  is the Boltzmann constant. The entropy associated to this distribution depends entirely on  $\{f_i\}$ :

$$S[\{f_i\}] = -k_B \sum_i [f_i \ln f_i + (1 - f_i) \ln(1 - f_i)]. \quad (5)$$

The Helmholtz free energy functional combines the KS energy and the entropy in a single functional defined as

$$A[T; \{\epsilon_i\}, \{|\psi_i\rangle\}] = \sum_i f_i \langle \psi_i | \hat{T} + \hat{V}_{ext} | \psi_i \rangle + E_H[n] + E_{XC}[n] - TS[\{f_i\}], \quad (6)$$

where  $E_H[n]$  and  $E_{XC}[n]$  are the Hartree energy and the exchange-correlation energies, respectively. Since the occupancies  $\{f_i\}$  are calculated as a function of  $\{\epsilon_i\}$ , the Helmholtz free energy,  $A[T; \{\epsilon_i\}, \{|\psi_i\rangle\}]$ , is considered to be a functional of  $\{\epsilon_i\}$  and  $\{|\psi_i\rangle\}$  only.

## III. IMPLEMENTATION IN ONETEP

In the implementation in ONETEP,<sup>24</sup> a finite set of  $N_b$  energy bands,  $\{|\psi_i\rangle\}$ , are expanded in terms of a set of  $N_b$  linearly independent NGWFs,<sup>51</sup>  $\{|\phi_\alpha\rangle\}$ , as

$$|\psi_i\rangle = |\phi_\alpha\rangle M_i^\alpha, \quad (7)$$

where  $\{M_i^\alpha\}$  are the expansion coefficients. The Einstein summation convention over repeated Greek indices is assumed. The elements of the overlap matrix corresponding to  $\{|\phi_\alpha\rangle\}$  are calculated with the inner product

$$S_{\alpha\beta} = \langle \phi_\alpha | \phi_\beta \rangle = \int d\mathbf{r} \phi_\alpha^*(\mathbf{r}) \phi_\beta(\mathbf{r}), \quad (8)$$

while the elements of the inverse overlap matrix  $\{S^{\alpha\beta}\}$  are obtained using an iterative technique.<sup>55</sup> Left-multiplying Eq. (7) with  $\langle \phi_\beta |$  and re-ordering terms, it follows:

$$M_i^\alpha = S^{\alpha\beta} \langle \phi_\beta | \psi_i \rangle. \quad (9)$$

Equation (7) can be seen as a change of representation from  $\{|\psi_i\rangle\}$ , in which the Hamiltonian  $\hat{H}$  is diagonal, to  $\{|\phi_\alpha\rangle\}$ , in which  $\hat{H}$  is not diagonal. The transformation generated by  $\{M_i^\alpha\}$  is not unitary as it transforms from an orthonormal to a non-orthogonal representation. The KS equations are written in the NGWF representation as

$$H_{\alpha\beta} M_i^\beta = S_{\alpha\beta} M_i^\beta \epsilon_i, \quad (10)$$

where  $\{H_{\alpha\beta}\}$  are the elements of the Hamiltonian matrix, defined as

$$H_{\alpha\beta} = \langle \phi_\alpha | \hat{H} | \phi_\beta \rangle = S_{\alpha\gamma} \sum_i^{N_b} (M_i^\gamma \epsilon_i M_i^{\dagger\delta}) S_{\delta\beta}. \quad (11)$$

Equation (10) corresponds to a set of  $N_b$  eigenvalue problems which are entirely defined if  $\{H_{\alpha\beta}\}$  and  $\{|\phi_\alpha\rangle\}$  are known. The eigenvalues  $\{\epsilon_i\}$  and the eigenvectors  $\{M_i^\alpha\}$  can be obtained simultaneously with an explicit diagonalization of the Hamiltonian matrix. The occupancies  $\{f_i\}$  are calculated as a function of  $\{\epsilon_i\}$  using Eq. (4). Therefore, the Helmholtz free energy becomes a functional of  $\{H_{\alpha\beta}\}$  and  $\{|\phi_\alpha\rangle\}$ :

$$A[T; \{H_{\alpha\beta}\}, \{|\phi_\alpha\rangle\}] = K^{\alpha\beta} \langle \phi_\beta | \hat{T} + \hat{V}_{ext} | \phi_\alpha \rangle + E_H[n] + E_{XC}[n] - TS[\{f_i\}], \quad (12)$$

where  $\{K^{\alpha\beta}\}$  are the elements of the density kernel matrix, defined as

$$K^{\alpha\beta} = \sum_i^{N_b} M_i^\alpha f_i M_i^{\dagger\beta}. \quad (13)$$

The electronic density is written in the NGWF representation as

$$n(\mathbf{r}) = \phi_\alpha(\mathbf{r}) K^{\alpha\beta} \phi_\beta^*(\mathbf{r}). \quad (14)$$

The NGWFs  $\{|\phi_\alpha\rangle\}$  are represented in real space as a linear combination of  $N_p$  psinc functions,  $\{D_p(\mathbf{r})\}$ , centered on the points with coordinates  $\{\mathbf{r}_p\}$  of a uniform computational grid:<sup>52</sup>

$$\phi_\alpha(\mathbf{r}) = \sum_{p=1}^{N_p} D_p(\mathbf{r}) c_{p\alpha}, \quad (15)$$

where  $\{c_{p\alpha}\}$  are the coefficients of the linear expansion. The psinc functions are related to plane-waves via a unitary transformation, and the basis set resolution can be systematically controlled by varying the plane-wave kinetic energy cutoff.<sup>52</sup> The core electrons are described with norm-conserving pseudopotentials. The NGWFs  $\{|\phi_\alpha\rangle\}$  are constrained to be strictly localized in real space within spheres of radii  $R_\alpha$  centered on the atomic nuclei.<sup>51</sup> Strict localization is maintained by constraining the coefficients  $\{c_{p\alpha}\}$  to be zero outside the localization spheres. This is a well-controlled approximation, in the sense that the description of the problem with localized NGWFs converges to the description with fully delocalized orbitals in the limit of increasingly large radii.<sup>47,48</sup>

The force acting on an atom  $I$  at the KS ground state is the derivative of the free energy functional with respect to the position vector of the nucleus of that atom,  $\mathbf{R}_I$ . The total force is equal to the sum of the Hellmann-Feynman<sup>56–58</sup> and Pulay terms:<sup>59,60</sup>

$$\mathbf{F}_I = \langle \phi_\alpha | \frac{\partial \hat{H}}{\partial \mathbf{R}_I} | \phi_\beta \rangle + \langle \frac{\partial \phi_\alpha}{\partial \mathbf{R}_I} | \hat{H} | \phi_\beta \rangle + \langle \phi_\alpha | \hat{H} | \frac{\partial \phi_\beta}{\partial \mathbf{R}_I} \rangle. \quad (16)$$

Many studies<sup>61–63</sup> prove that there is no extra term due to the fractional occupancies or the entropy term if the occupancies follow the Fermi-Dirac distribution.

## IV. DIRECT FREE ENERGY MINIMIZATION

The approach to minimize the Helmholtz free energy functional presented in this work consists of two nested loops, following the Ensemble-DFT method developed by Marzari *et al.*<sup>44</sup> First, the inner loop minimizes  $A[T; \{H_{\alpha\beta}\}, \{|\phi_\alpha\rangle\}]$  with respect to  $\{H_{\alpha\beta}\}$ , for a constant set of  $\{|\phi_\alpha\rangle\}$ .<sup>45</sup> Once the inner loop is finished, an outer loop minimizes a projected functional

$$A'[T; \{|\phi_\alpha\rangle\}] = \min_{\{H_{\alpha\beta}\}} A[T; \{H_{\alpha\beta}\}, \{|\phi_\alpha\rangle\}] \quad (17)$$

with respect to  $\{|\phi_\alpha\rangle\}$ . Both the inner and outer loop use a self-consistent direct minimization approach that ensures convergence towards the KS ground-state at every step and completely removes charge sloshing effects.<sup>64</sup>

### A. Inner loop

For the inner loop, the method developed by Freysoldt *et al.*,<sup>45</sup> based on a line-search algorithm in the space of non-diagonal Hamiltonian elements,  $\{H_{\alpha\beta}\}$  was found to offer significant numerical benefits. An approach of this type ensures that only the Hamiltonian matrix has to be diagonalized. The eigenspectra of  $\{H_{\alpha\beta}\}$  (the set of energy eigenvalues  $\{\epsilon_i\}$ ) is not compressed within a particular range of real values, and degenerate states appear in few subgroups which are orthonormal to each other. Reorthonormalizing each subgroup independently does not require extensive computational resources and makes the process suitable for large calculations with parallel eigensolvers. Also, such an algorithm allows the occupancies to be calculated from the energy eigenvalues, and not the other way around. Therefore, the aufbau principle holds at all times.

At iteration  $m$  of the inner loop, the Hamiltonian matrix is first diagonalized as

$$H_{\alpha\beta}^{(m)} M_i^{\beta(m)} = S_{\alpha\beta} M_i^{\beta(m)} \epsilon_i^{(m)}, \quad (18)$$

after which degenerate eigenstates are orthonormalized with the Löwdin symmetric orthonormalization method.<sup>65</sup> The occupancies  $\{f_i^{(m)}\}$  are calculated using Eq. (4), and the entropy term  $S^{(m)}$  is calculated from  $\{f_i^{(m)}\}$  using Eq. (5). The new density kernel is built as

$$K^{\alpha\beta(m)} = \sum_i^{N_b} M_i^{\alpha(m)} f_i^{(m)} M_i^{\dagger\beta(m)}, \quad (19)$$

and the electronic density  $n^{(m)}(\mathbf{r})$  is updated as

$$n^{(m)}(\mathbf{r}) = \phi_\alpha(\mathbf{r}) K^{\alpha\beta(m)} \phi_\beta^*(\mathbf{r}). \quad (20)$$

The density-dependent components of the Hamiltonian  $\hat{V}_H[n^{(m)}]$  and  $\hat{V}_{XC}[n^{(m)}]$  are updated and the Helmholtz free energy functional  $A^{(m)}$  is evaluated. A new Hamiltonian matrix of elements  $\{\tilde{H}_{\alpha\beta}^{(m)}\}$  is constructed as

$$\tilde{H}_{\alpha\beta}^{(m)} = \langle \phi_\alpha | \hat{T} + \hat{V}_{ext} + \hat{V}_H[n^{(m)}] + \hat{V}_{XC}[n^{(m)}] | \phi_\beta \rangle. \quad (21)$$

The values of  $\{\tilde{H}_{\alpha\beta}^{(m)}\}$  are used to define a search direction  $\{\Delta_{\alpha\beta}^{(m)}\}$  in the multidimensional space of non-diagonal

Hamiltonian matrix elements as

$$\Delta_{\alpha\beta}^{(m)} = \tilde{H}_{\alpha\beta}^{(m)} - H_{\alpha\beta}^{(m)}. \quad (22)$$

The Hamiltonian matrix  $H_{\alpha\beta}^{(m)}$  is updated as

$$H_{\alpha\beta}^{(m+1)} = H_{\alpha\beta}^{(m)} + \lambda \Delta_{\alpha\beta}^{(m)}. \quad (23)$$

The choice of this search direction is similar to the choice of search directions in the algorithms by Marzari *et al.*<sup>44</sup> and Freysoldt *et al.*<sup>45</sup> The above equation can be recast into  $H_{\alpha\beta}^{(m+1)} = (1 - \lambda)H_{\alpha\beta}^{(m)} + \lambda\tilde{H}_{\alpha\beta}^{(m)}$ , where  $\lambda$  acts as an optimal damping parameter that has been chosen with the purpose of minimizing the free energy functional. The parameter  $\lambda$  is calculated using a second-order polynomial fitting of the free energy functional after evaluating  $A[\mathbf{T}; \{H_{\alpha\beta}\}, \{|\phi_{\alpha}\rangle\}]$  along the search direction  $\Delta_{\alpha\beta}^{(m)}$  at  $\lambda = 0$  and at two trial steps in the range  $[0, 1]$ . Occasionally, in the very first iterations, a third-order polynomial fitting may be required. Rarely, a fourth-order polynomial can be necessary. The algorithm quickly falls into the parabolic regime. The minimum is reached when the commutator  $[H_{\alpha\beta}^{(m+1)}, K^{\alpha\beta(m)}]$ , which is zero at self-consistency, falls below the pre-selected tolerance threshold. Typically, 3–5 inner loop iterations are required per outer loop iteration.

## B. Outer loop

The outer loop optimizes  $\{|\phi_{\alpha}\rangle\}$ ,<sup>47–51</sup> with fixed  $\{H_{\alpha\beta}\}$  by minimizing the projected free energy functional  $A'[\mathbf{T}; \{|\phi_{\alpha}\rangle\}]$ . At iteration  $l$  of the outer loop, the derivative of  $A^{(l)}$  with respect to  $\langle\phi_{\beta}^{(l)}|$  is

$$|\Gamma^{\beta(l)}\rangle = \frac{\delta A^{(l)}}{\delta \langle\phi_{\beta}^{(l)}|} = \hat{H}^{(l)} |\phi_{\gamma}^{(l)}\rangle K^{\gamma\beta}. \quad (24)$$

Orthonormality of the KS states  $\{|\psi_i\rangle\}$ , as described by the NGWFs, can be imposed to first order by projecting out the components of  $|\Gamma^{\beta(l)}\rangle$  that are parallel to all  $|\phi_{\gamma}^{(l)}\rangle$ , resulting in the expression<sup>3,66</sup>

$$|\tilde{\Gamma}^{\beta(l)}\rangle = \hat{H}^{(l)} |\phi_{\gamma}^{(l)}\rangle K^{\gamma\beta} - |\phi_{\gamma}^{(l)}\rangle K^{\gamma\delta} H_{\delta\nu}^{(l)} S^{\nu\beta(l)}. \quad (25)$$

The covariant tensorial nature of the NGWFs<sup>67</sup> is taken into account by right-multiplying Eq. (25) with  $S_{\beta\alpha}^{(l)}$ , leading to

$$|\tilde{\Gamma}_{\alpha}^{(l)}\rangle = \hat{H}^{(l)} |\phi_{\gamma}^{(l)}\rangle K^{\gamma\beta} S_{\beta\alpha}^{(l)} - |\phi_{\gamma}^{(l)}\rangle K^{\gamma\delta} H_{\delta\alpha}^{(l)}. \quad (26)$$

Occupancy<sup>44</sup> and kinetic energy preconditioning<sup>68</sup> can be applied to  $|\tilde{\Gamma}_{\alpha}^{(l)}\rangle$ , resulting in

$$|\tilde{\Delta}_{\alpha}^{(l)}\rangle = -\hat{P}[\hat{H}^{(l)} |\phi_{\alpha}^{(l)}\rangle - |\phi_{\beta}^{(l)}\rangle S^{\beta\gamma(l)} H_{\gamma\alpha}^{(l)}], \quad (27)$$

where  $\hat{P}$  is a generic kinetic energy preconditioning operator<sup>3</sup> and the leading minus is a consequence of the “downhill” update of the steepest descent method. The vector  $|\tilde{\Delta}_{\alpha}^{(l)}\rangle$  does not yet account for the localization constraint of the NGWFs.  $|\tilde{\Delta}_{\alpha}^{(l)}\rangle$  is represented in the psinc basis set as

$$\tilde{\Delta}_{\alpha}^{(l)}(\mathbf{r}) = \sum_{p=1}^{N_p} D_p(\mathbf{r}) \tilde{d}_{p\alpha}^{(l)}, \quad (28)$$

where  $\{\tilde{d}_{p\alpha}^{(l)}\}$  are the expansion coefficients. The non-zero elements corresponding to grid points outside the localization sphere are projected out as

$$d_{p\alpha}^{(l)} = \begin{cases} \tilde{d}_{p\alpha}^{(l)}, & |\mathbf{R}_{\alpha} - \mathbf{r}_p| < R_{\alpha} \\ 0, & |\mathbf{R}_{\alpha} - \mathbf{r}_p| \geq R_{\alpha}. \end{cases} \quad (29)$$

The resulting vectors  $|\Delta_{\alpha}^{(l)}\rangle$  are the steepest descent search directions, represented in terms of the psinc basis set as

$$\Delta_{\alpha}^{(l)}(\mathbf{r}) = \sum_{p=1}^{N_p} D_p(\mathbf{r}) d_{p\alpha}^{(l)}. \quad (30)$$

The conjugate gradients search direction  $|\chi_{\alpha}^{(l)}\rangle$  is obtained by conjugating  $|\Delta_{\alpha}^{(l)}\rangle$  to  $|\chi_{\alpha}^{(l-1)}\rangle$ :

$$|\chi_{\alpha}^{(l)}\rangle = |\Delta_{\alpha}^{(l)}\rangle + \frac{\langle\tilde{\Gamma}^{\beta(l)}|\Delta_{\alpha}^{(l)}\rangle}{\langle\tilde{\Gamma}^{\gamma(l-1)}|\chi_{\gamma}^{(l-1)}\rangle} |\chi_{\alpha}^{(l-1)}\rangle. \quad (31)$$

Convergence of the outer loop is judged by monitoring the slope along the search direction  $\langle\tilde{\Gamma}^{\alpha(l)}|\chi_{\alpha}^{(l)}\rangle$ , which is zero at self-consistency, indicating that the minimum along the trajectory in the free energy surface compatible with the constraint of localization of  $\{|\phi_{\alpha}\rangle\}$  has been reached. If self-consistency is not yet achieved, the NGWFs are updated as

$$|\phi_{\alpha}^{(l+1)}\rangle = |\phi_{\alpha}^{(l)}\rangle + \eta |\chi_{\alpha}^{(l)}\rangle, \quad (32)$$

where  $\eta$  is the optimal step-length obtained using a second-order polynomial fitting of  $A'[\mathbf{T}; \{|\phi_{\alpha}\rangle\}]$  along the search direction  $|\chi_{\alpha}^{(l)}\rangle$  (a third-order polynomial fitting is rarely needed). The algorithm continues by updating the overlap and inverse overlap matrices  $\{S_{\alpha\beta}^{(l+1)}\}$  and  $\{S^{\alpha\beta(l+1)}\}$ , respectively. The transformation  $\{M_i^{\alpha}\}$  must be represented in terms of the new NGWFs,  $\{|\phi_{\alpha}^{(l+1)}\rangle\}$ , for consistency. Combining the closure relation

$$\hat{I} = |\phi_{\alpha}^{(l+1)}\rangle S^{\alpha\beta(l+1)} \langle\phi_{\beta}^{(l+1)}| \quad (33)$$

and the expansion of the KS states in terms of the previous NGWF representation

$$|\psi_i\rangle = |\phi_{\alpha}^{(l)}\rangle M_i^{\alpha}, \quad (34)$$

it is obtained that

$$\tilde{M}_i^{\alpha} = S^{\alpha\beta(l+1)} \langle\phi_{\beta}^{(l+1)}|\phi_{\gamma}^{(l)}\rangle M_i^{\gamma}. \quad (35)$$

The density kernel is rebuilt as

$$\tilde{K}^{\alpha\beta} = \sum_i^{N_b} \tilde{M}_i^{\alpha} f_i \tilde{M}_i^{\beta}, \quad (36)$$

followed by the update of the electronic density:

$$n^{(l+1)}(\mathbf{r}) = \phi_{\alpha}^{(l+1)}(\mathbf{r}) \tilde{K}^{\alpha\beta} \phi_{\beta}^{*(l+1)}(\mathbf{r}), \quad (37)$$

and the density-dependent terms  $\hat{V}_H[n^{(l+1)}]$  and  $\hat{V}_{XC}[n^{(l+1)}]$ . The projected functional  $A^{(l+1)}$  is evaluated, following the update of the Hamiltonian before re-entering the inner loop. The two-nested-loop approach is repeated to self-consistency until convergence to the desired tolerance threshold is achieved.

## V. RESULTS AND DISCUSSION

### A. Scaling with the system size

A key feature of the approach presented in this work is the use of NGWFs. As a consequence of the strict spherical localization constraints imposed on  $\{\phi_\alpha\}$ , most of the overlap  $\{S_{\alpha\beta}\}$  and Hamiltonian  $\{H_{\alpha\beta}\}$  matrix elements are zero. Therefore, both matrices are sparse, allowing the custom-built, highly parallel, optimized sparse algebra routines included in the ONETEP program<sup>53</sup> to be utilized. The cost of algebraic operations with sparse matrices scales as  $\mathcal{O}(N)$  with the number of the atoms in the system,  $N$ . Additionally, the cost of fast Fourier transforms (FFTs) also scales as  $\mathcal{O}(N)$  with the use of the FFT-box technique.<sup>52,69</sup> As a result, many essential steps of the algorithm such as updating the electronic density on a grid, updating the Hamiltonian elements, or calculating the NGWF gradient can be performed at  $\mathcal{O}(N)$  cost (linear-scaling).

However, the computational cost and memory requirements to diagonalize the Hamiltonian is  $\mathcal{O}(N^3)$ . Therefore, the overall scaling of the algorithm is also  $\mathcal{O}(N^3)$  (cubic-scaling). The strategy followed in this work is not of avoiding the diagonalization step, but rather of reducing its impact on performance. The NGWFs are essential to this goal. The set of  $\{\phi_\alpha\}$  contains a minimal number of functions which are used to represent the Hamiltonian operator. Hence, the Hamiltonian matrix to be diagonalized is reduced to have the smallest possible dimensions, which reduces the prefactor associated to diagonalization and its impact on the total runtime of the algorithm. Chemical accuracy is achieved by means of optimizing the NGWFs in the psinc basis set during the outer loop at  $\mathcal{O}(N)$  cost. The memory requirements are often a stronger limiting factor than the computational time. This is due to the fact that  $\{M_i^\alpha\}$ ,  $\{K^{\alpha\beta}\}$ , and other temporary matrices are dense, amounting for  $(N_b \times N)^2$  non-zero elements per matrix that must be stored. In order to be able to simulate large systems with thousand of atoms, memory storage of matrix elements has to be shared over multiple cores. To address this difficulty, the ScaLAPACK PDSYGVX parallel eigensolver<sup>54</sup> was used, not only to accelerate the diagonalization step with parallel algebra techniques, but more importantly, to divide and distribute the matrix elements over the memory of a large number of cores in an efficient way.<sup>50</sup>

To demonstrate the computational demands of some of the most relevant parts of the algorithm, a set of benchmark calculations on Au cuboctahedral nanoparticles of increasing size, ranging between 309 and 2057 atoms, was performed. All the calculations were run on 120 cores distributed over 20 6-core 2.4 GHz Intel Westmere processors and 3.6 GB of memory per core. The calculations use a NGWF radii of  $R_\alpha = 5.0$  Å, a kinetic energy cut-off of 700 eV, an electronic smearing of  $k_B T = 0.1$  eV, the Perdew-Burke-Ernzerhof (PBE) exchange-correlation functional,<sup>70</sup> and a norm-conserving pseudopotential with 11 valence electrons per atom. Figure 1 shows the time per one outer loop iteration with five inner loop iterations compared to the system size, given by the number of atoms. The inset plot shows the number of non-zero matrix elements  $\{S_{\alpha\beta}\}$  and  $\{H_{\alpha\beta}\}$  in each calculation. The number of non-zero  $\{S_{\alpha\beta}\}$  and  $\{H_{\alpha\beta}\}$

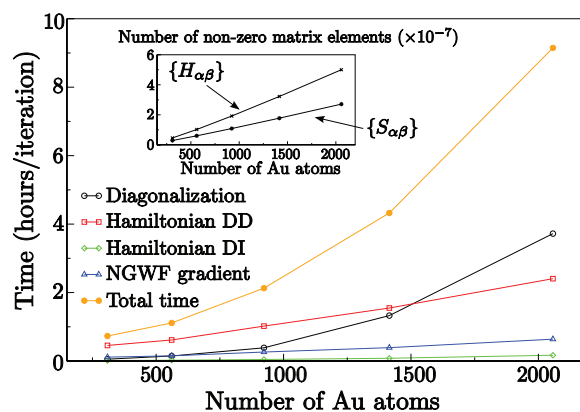


FIG. 1. Time taken to complete one outer loop iteration with five inner loop iterations, in calculations on Au nanoparticles of increasing size. The plot shows the time taken by different parts of the algorithm. “Hamiltonian DD” and “Hamiltonian DI” must be interpreted as the density-dependent and density-independent terms of the Hamiltonian, respectively.

matrix elements scales linearly with the number of atoms, and both matrices remain sparse regardless of the size of the system. The fact that the Hamiltonian matrix is less sparse compared to the overlap matrix is due to the non-local part of the norm-conserving pseudopotential.<sup>69</sup> Algebraic operations that involve these two matrices can be carried out at a linear-scaling cost using parallel sparse algebra methods.<sup>53</sup> The time to execute critical steps of the algorithm such as building the density-independent and density-dependent terms of the Hamiltonian matrix (including updating the electronic density) and calculating the NGWF gradient scale linearly with the number of atoms. For small systems, building the density-dependent terms of the Hamiltonian is the most computationally demanding part of the calculation. As the number of atoms increases, diagonalization becomes more costly, and rapidly claims most of the computational effort at every iteration. In calculations of 1500 atoms and above, diagonalizing the Hamiltonian is the most expensive part of the calculation. Eventually, the cost of diagonalization will limit the size of systems that can be simulated.

### B. Validation tests

A number of validation calculations were completed in order to test the accuracy of the method. In all the calculations shown hereafter the RMS commutator  $[H_{\alpha\beta}, K^{\alpha\beta}]$  was converged within a tolerance of at least  $1 \times 10^{-4}$  eV, while the RMS of the slope of the NGWF gradient along the search direction,  $\langle \Gamma^\alpha | \chi_\alpha \rangle$ , was converged to at least  $5 \times 10^{-5}$  eV. With these settings, the free energy functional is converged below  $10^{-6}$  eV/atom in all cases. First, Broyden-Fletcher-Goldfarb-Shanno (BFGS) geometry optimization calculations<sup>71</sup> on a Pt<sub>13</sub> cuboctahedral nanoparticle were performed. The results were compared to those obtained with the finite-temperature KS-DFT direct minimization method included in CASTEP,<sup>4</sup> which uses fully delocalized orbitals and a plane-waves basis set. The calculations with the two programs use the same settings: a kinetic energy cut-off of 1000 eV, an electronic smearing of  $k_B T = 0.1$  eV,

TABLE I. BFGS geometry optimization of Pt<sub>13</sub> with ONETEP and CASTEP. The table shows the optimized value of the distance to the nearest-neighbour Pt atom.

	Distance (Å)
ONETEP ( $R_\alpha = 3.0$ Å)	2.64
ONETEP ( $R_\alpha = 3.5$ Å)	2.66
ONETEP ( $R_\alpha = 4.0$ Å)	2.69
ONETEP ( $R_\alpha = 4.5$ Å)	2.69
ONETEP ( $R_\alpha = 5.0$ Å)	2.69
ONETEP ( $R_\alpha = 5.5$ Å)	2.70
ONETEP ( $R_\alpha = 6.0$ Å)	2.70
CASTEP	2.70

the PBE exchange-correlation functional,<sup>70</sup> the same set of norm-conserving pseudopotentials with 10 valence electrons per atom, and a total of 117 energy bands. In the calculations with ONETEP, 9 NGWFs are assigned per atom. The optimized structures obtained with NGWF radii in the range 3.0 Å–6.0 Å were compared. Table I shows the final value of the distance to the nearest-neighbour Pt atom. Convergence of the optimized geometry to a single structure is achieved as  $R_\alpha$  increases. The structures obtained with ONETEP match the result obtained with CASTEP within 0.01 Å tolerance for  $R_\alpha = 4.0$  Å and above. The density of states (DOS) of the optimized structures, calculated with a Gaussian smearing of 0.1 eV, is shown in Fig. 2. The DOS obtained with ONETEP also matches the CASTEP results for  $R_\alpha = 4.0$  Å and above, in the region of energies below and in the vicinity of the Fermi level  $\mu$ . The ONETEP DOS is known to be inaccurate to describe the higher-energy, near-empty bands above the Fermi level, unless the conduction bands are optimized further.<sup>72</sup>

The next validation test involved calculations on face-centered cubic (fcc) bulk Cu. The free energy potential associated with variations in the lattice parameter was obtained with ONETEP and compared against the potential obtained with CASTEP. The ONETEP calculations include only the  $\Gamma$ -point. In order to imitate the behavior of the k-point grid, at least to some extent, the four-atom fcc cell of bulk Cu was replicated five times in each lattice vector

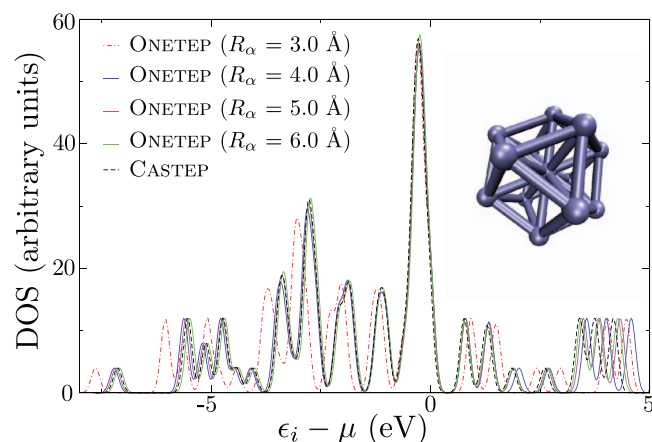


FIG. 2. Density of states of Pt<sub>13</sub> obtained with ONETEP and CASTEP. Agreement is achieved for NGWF radii of 4.0 Å and above.

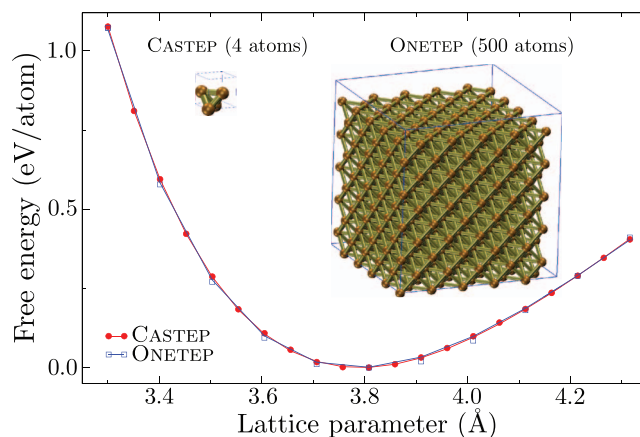


FIG. 3. Lattice parameter stretching of bulk Cu. There are 4 atoms in the CASTEP simulation cell and 500 atoms in the ONETEP simulation cell, forming a  $5 \times 5 \times 5$  supercell.

direction, resulting in a  $5 \times 5 \times 5$  supercell containing 500 atoms. The procedure described in Ref. 73 to vary the lattice parameter while maintaining the kinetic energy cut-off constant in the ONETEP calculations was used. The settings in both programs are the same: a kinetic energy cut-off of 898.2 eV, an electronic smearing of  $k_B T = 0.1$  eV, the revised Perdew-Burke-Ernzerhof exchange-correlation functional,<sup>74</sup> and the same norm-conserving pseudopotentials with 11 valence electrons per atom. In ONETEP, each Cu atom was assigned 9 NGWFs of radii  $R_\alpha = 4.0$  Å, amounting for a total of 4500 energy bands in the system. The CASTEP calculations include one four-atom fcc cell, a Monkhorst-Pack k-point grid<sup>75</sup> of 5 points in each direction, and a total of 27 energy bands in the system. The results are shown in Fig. 3. The bulk modulus  $B$  and the equilibrium lattice parameter  $L_0$  were calculated by fitting a curve determined by the third-order Birch-Murnaghan equation<sup>76</sup> to the results. These are shown in Table II. The calculations with CASTEP and ONETEP agree very well in their predictions of  $L_0$  (within 0.01 Å) and  $B$  (within 0.06 GPa). These results on bulk Cu confirm that a similar level of accuracy in the description of crystalline systems can be achieved compared to standard KS-DFT methods. More importantly, these calculations exemplify how calculations on periodic systems with hundreds of atoms in the simulation cell can be performed with the algorithm presented in this work. This capability can be used to study complicated periodic structures formed by many atoms in one, two, or three dimensions, or with many lattice defects. Amorphous systems could also be studied in closer detail by allowing more atoms in the simulation cell.<sup>35,36</sup>

TABLE II. Bulk modulus,  $B$ , and equilibrium lattice parameter,  $L_0$ , of bulk Cu, calculated with CASTEP and ONETEP. The value of  $\chi^2$  corresponding to the fitting of the results to the third-order Birch-Murnaghan equation is also shown.

	$B$ (GPa)	$L_0$ (Å)	$\chi^2$
CASTEP	93.57	3.79	$6 \times 10^{-5}$
ONETEP	93.51	3.79	$6 \times 10^{-4}$

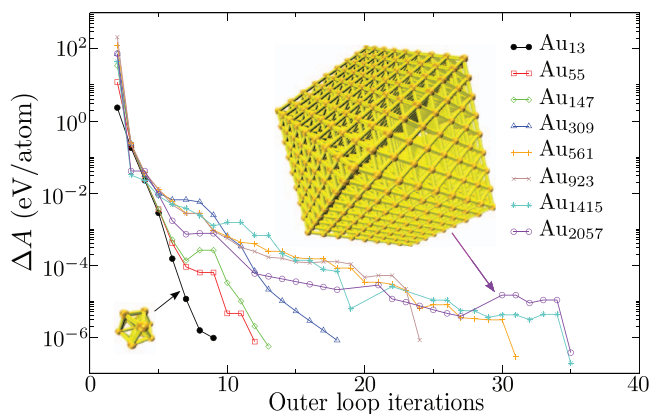


FIG. 4. Convergence of the Helmholtz free energy functional of the number of outer loop (NGWF optimization) iterations, for a set of Au cuboctahedral nanoparticles of increasing sizes. The structures of Au<sub>13</sub> and Au<sub>2057</sub> are also shown in the plot.

The last set of tests aims to provide an insight into the capabilities of the algorithm to successfully complete calculations on metallic systems that can be of practical use on industrial processes. A series of calculations on isolated Au cuboctahedral nanoparticles of different sizes, from 0.4 to 3.4 nm wide, in the range of 13–2057 atoms, were performed. These kind of nanoparticles are of interest for the development of novel catalysts, but their large sizes make computational studies with KS-DFT expensive. Recent studies have reported that 32 768 cores were required to perform calculations on Au<sub>1415</sub> using standard plane-waves KS-DFT methods.<sup>29</sup>

The calculations with ONETEP use the same configuration as in the calculations shown in Fig. 1. Convergence is achieved when the change in the free energy per atom is less than  $10^{-6}$  eV and the RMS gradient along the NGWF search direction falls below  $2 \times 10^{-5}$  eV. All the calculations converged within these tolerance thresholds. Figure 4 shows the convergence rate with number of outer loop iterations using ONETEP. To some extent, the number of iterations required is system-dependent and increases with the number of atoms. The largest of the Au nanoparticles, containing 2057 atoms, converged within 240 h using 300 cores distributed across 25 12-core 2.4 GHz Intel Westmere processors with 1.8 GB of memory per core. Provided there are enough computational resources, the method presented in this work could enable calculations to study even larger industrial catalysts which typically consist of thousands of metallic atoms.<sup>31</sup>

## VI. CONCLUSIONS

In this work, an approach for finite-temperature KS-DFT on large metallic systems, based on direct minimization of the Helmholtz free energy functional, was presented. In its implementation within the ONETEP program, the cost of most parts of the calculation is reduced to the linear-scaling regime. This is due to the use of localized orbitals which are optimized *in situ* in terms of a periodic-sinc basis set. The impact of Hamiltonian diagonalization, which remains cubic-scaling, is reduced to the minimum. Parallel eigensolvers are used to dis-

tribute the memory requirements over many cores in an efficient manner.

This approach was validated by comparing the results of calculations on a small Pt nanoparticle and in bulk Cu with those obtained with the CASTEP code, which uses delocalized orbitals and plane-waves. In both cases, a very good agreement of the electronic and structural properties was shown. Further calculations carried on to completion on Au nanoparticles with up to 2057 atoms demonstrate that this approach is able to perform calculations on metallic systems with thousands of atoms. Such capability has the potential to expand the range of metallic compounds that can be studied with finite-temperature Kohn-Sham DFT and to allow simulations of larger nanoparticles or alloys with direct industrial relevance.

## ACKNOWLEDGMENTS

A.R.-S. acknowledges the support of the Engineering and Physical Sciences Research Council (EPSRC) (Grant No. EP/F038038/1) for a High End Computing Studentship through the UKCP consortium. C.-K.S. acknowledges support from the Royal Society in the form of a University Research Fellowship. The authors are grateful for the computing resources provided by Southampton University's iSolutions unit (Iridis3 supercomputer) which have enabled all the calculations presented here.

- <sup>1</sup>P. Hohenberg and W. Kohn, *Phys. Rev.* **136**, B864 (1964).
- <sup>2</sup>W. Kohn and L. J. Sham, *Phys. Rev.* **140**, A1133 (1965).
- <sup>3</sup>M. C. Payne, M. P. Teter, D. C. Allan, T. A. Arias, and J. D. Joannopoulos, *Rev. Mod. Phys.* **64**, 1045 (1992).
- <sup>4</sup>S. J. Clark, M. D. Segall, C. J. Pickard, P. J. Hasnip, M. J. Probert, K. Refson, and M. C. Payne, *Z. Kristallogr. Kristallgeom. Kristallphys.* **220**, 567 (2005).
- <sup>5</sup>G. Kresse and J. Furthmüller, *Phys. Rev. B* **54**, 11169 (1996).
- <sup>6</sup>P. Giannozzi, S. Baroni, N. Bonini, M. Calandra, R. Car, C. Cavazzoni, D. Ceresoli, G. L. Chiarotti, M. Cococcioni, I. Dabo, A. dal Corso, S. de Gironcoli, S. Fabris, G. Fratesi, R. Gebauer, U. Gerstmann, C. Gougousis, A. Kokalj, M. Lazzeri, L. Martin-Samos, N. Marzari, F. Mauri, R. Mazzarello, S. Paolini, A. Pasquarello, L. Paulatto, C. Sbraccia, S. Scandolo, G. Sclauzero, A. P. Seitsonen, A. Smogunov, P. Umari, and R. M. Wentzcovitch, *J. Phys. Condens. Matter* **21**, 395502 (2009).
- <sup>7</sup>X. Gonze, B. Amadon, P. M. Anglade, J. M. Beuken, F. Bottin, P. Boulanger, F. Bruneval, D. Caliste, R. Caracas, M. Cote, T. Deutsch, L. Genovese, P. Ghosez, M. Giantomassi, S. Goedecker, D. R. Hamann, P. Hermet, F. Jollet, G. Jomard, S. Leroux, M. Mancini, S. Mazevet, M. J. T. Oliveira, G. Onida, Y. Pouillon, T. Rangel, G. M. Rignanese, D. Sangalli, R. Shaltaf, M. Torrent, M. J. Verstraete, G. Zerah, and J. W. Zwanziger, *Comput. Phys. Commun.* **180**, 2582 (2009).
- <sup>8</sup>J. Enkovaara, C. Rostgaard, J. J. Mortensen, J. Chen, M. Dułak, L. Ferrighi, J. Gavnholt, C. Glinsvad, V. Haikola, H. A. Hansen, H. H. Kristoffersen, M. Kuisma, A. H. Larsen, L. Lehtovaara, M. Ljungberg, O. Lopez-Acevedo, P. G. Moses, J. Ojanen, T. Olsen, V. Petzold, N. A. Romero, J. Stausholm-Møller, M. Strange, G. A. Tritsarlis, M. Vanin, M. Walter, B. Hammer, H. Häkkinen, G. K. H. Madsen, R. M. Nieminen, J. K. Nørskov, M. Puska, T. T. Rantala, J. Schiøtz, K. S. Thygesen, and K. W. Jacobsen, *J. Phys. Condens. Matter* **22**, 253202 (2010).
- <sup>9</sup>P. E. Blöchl, *Phys. Rev. B* **50**, 17953 (1994).
- <sup>10</sup>E. R. Davidson and D. Feller, *Chem. Rev.* **86**, 681 (1986).
- <sup>11</sup>P. R. Briddon and R. Jones, *Phys. Status Solidi B* **217**, 131 (2000).
- <sup>12</sup>M. Valiev, E. J. Bylaska, N. Govind, K. Kowalski, T. P. Straatsma, H. J. J. van Dam, D. Wang, J. Nieplocha, E. Apra, T. L. Windus, and W. A. de Jong, *Comput. Phys. Commun.* **181**, 1477 (2010).
- <sup>13</sup>G. te Velde, F. M. Bickelhaupt, E. J. Baerends, C. Fonseca Guerra, S. J. A. van Gisbergen, J. G. Snijders, and T. Ziegler, *J. Comput. Chem.* **22**, 931 (2001).
- <sup>14</sup>O. F. Sankey and D. J. Niklewski, *Phys. Rev. B* **40**, 3979 (1989).

- <sup>15</sup>E. Artacho, D. Sánchez-Portal, P. Ordejón, A. García, and J. M. Soler, *Phys. Status Solidi B* **215**, 809 (1999).
- <sup>16</sup>S. García-Gil, A. García, N. Lorente, and P. Ordejón, *Phys. Rev. B* **79**, 075441 (2009).
- <sup>17</sup>A. S. Torralba, M. Todorovic, V. Brazdova, R. Choudhury, T. Miyazaki, M. J. Gillan, and D. R. Bowler, *J. Phys. Condens. Matter* **20**, 294206 (2008).
- <sup>18</sup>M. Chen, G. C. Guo, and L. He, *J. Phys. Condens. Matter* **22**, 445501 (2010).
- <sup>19</sup>M. J. Louwerse and G. Rothenberg, *Phys. Rev. B* **85**, 035108 (2012).
- <sup>20</sup>V. Blum, R. Gehrke, F. Hanke, P. Havu, V. Havu, X. Ren, K. Reuter, and M. Scheffler, *Comput. Phys. Commun.* **180**, 2175 (2009).
- <sup>21</sup>S. Goedecker, *Rev. Mod. Phys.* **71**, 1085 (1999).
- <sup>22</sup>E. Prodan and W. Kohn, *Proc. Natl. Acad. Sci. U.S.A.* **102**, 11635 (2005).
- <sup>23</sup>W. Kohn, *Phys. Rev. Lett.* **76**, 3168 (1996).
- <sup>24</sup>C.-K. Skylaris, P. D. Haynes, A. A. Mostofi, and M. C. Payne, *J. Chem. Phys.* **122**, 084119 (2005).
- <sup>25</sup>M. J. Gillan, D. R. Bowler, A. S. Torralba, and T. Miyazaki, *Comput. Phys. Commun.* **177**, 14 (2007).
- <sup>26</sup>J. Soler, E. Artacho, J. Gale, A. Garcia, J. Junquera, P. Ordejón, and D. Sanchez-Portal, *J. Phys. Condens. Matter* **14**, 2745 (2002).
- <sup>27</sup>T. Ozaki and H. Kino, *Phys. Rev. B* **72**, 045121 (2005).
- <sup>28</sup>L. Genovese, A. Neelov, S. Goedecker, T. Deutsch, S. A. Ghasemi, A. Willand, D. Caliste, O. Zilberberg, M. Rayson, A. Bergman, and R. Schneider, *J. Chem. Phys.* **129**, 014109 (2008).
- <sup>29</sup>J. Kleis, J. Greeley, N. A. Romero, V. A. Morozov, H. Falsig, A. H. Larsen, J. Lu, J. J. Mortensen, M. Dulak, K. S. Thygesen, J. K. Nørskov, and K. W. Jacobsen, *Catal. Lett.* **141**, 1067 (2011).
- <sup>30</sup>L. Li, A. H. Larsen, N. A. Romero, V. A. Morozov, C. Glinsvad, F. Abild-Pedersen, J. Greeley, K. W. Jacobsen, and J. K. Nørskov, *J. Phys. Chem. Lett.* **4**, 222 (2013).
- <sup>31</sup>F. Baletto and R. Ferrando, *Rev. Mod. Phys.* **77**, 371 (2005).
- <sup>32</sup>B. G. Walker, N. Marzari, and C. Molteni, *J. Phys. Condens. Matter* **18**, L269 (2006).
- <sup>33</sup>R. Kavanagh, X. M. Cao, W. F. Lin, C. Hardacre, and P. Hu, *Angew. Chem., Int. Ed.* **51**, 1572 (2012).
- <sup>34</sup>Z. P. Liu and P. Hu, *J. Am. Chem. Soc.* **125**, 1958 (2003).
- <sup>35</sup>R. Ferrando, J. Jellinek, and R. L. Johnston, *Chem. Rev.* **108**, 845 (2008).
- <sup>36</sup>J. Oviedo and R. E. Palmer, *J. Chem. Phys.* **117**, 9548 (2002).
- <sup>37</sup>J. Hafner, *J. Comput. Chem.* **29**, 2044 (2008).
- <sup>38</sup>N. D. Mermin, *Phys. Rev.* **137**, A1441 (1965).
- <sup>39</sup>R. G. Parr and W. Yang, *Density-Functional Theory of Atoms and Molecules*, International Series of Monographs on Chemistry Vol. 16 (Oxford University Press, 1989).
- <sup>40</sup>P. Pulay, *Chem. Phys. Lett.* **73**, 393 (1980).
- <sup>41</sup>E. Cancès, K. N. Kudin, G. E. Scuseria, and G. Turinici, *J. Chem. Phys.* **118**, 5364 (2003).
- <sup>42</sup>M. J. Gillan, *J. Phys. Condens. Matter* **1**, 689 (1989).
- <sup>43</sup>M. P. Grumbach, D. Hohl, R. M. Martin, and R. Car, *J. Phys. Condens. Matter* **6**, 1999 (1994).
- <sup>44</sup>N. Marzari, D. Vanderbilt, and M. C. Payne, *Phys. Rev. Lett.* **79**, 1337 (1997).
- <sup>45</sup>C. Freysoldt, S. Boeck, and J. Neugebauer, *Phys. Rev. B* **79**, 241103 (2009).
- <sup>46</sup>G. Galli and M. Parrinello, *Phys. Rev. Lett.* **69**, 3547 (1992).
- <sup>47</sup>F. Mauri and G. Galli, *Phys. Rev. B* **50**, 4316 (1994).
- <sup>48</sup>P. Ordejón, D. A. Drabold, R. M. Martin, and M. P. Grumbach, *Phys. Rev. B* **51**, 1456 (1995).
- <sup>49</sup>E. Hernández and M. J. Gillan, *Phys. Rev. B* **51**, 10157 (1995).
- <sup>50</sup>J.-L. Fattebert and J. Bernholc, *Phys. Rev. B* **62**, 1713 (2000).
- <sup>51</sup>C.-K. Skylaris, A. A. Mostofi, P. D. Haynes, O. Dieguez, and M. C. Payne, *Phys. Rev. B* **66**, 035119 (2002).
- <sup>52</sup>C.-K. Skylaris, A. A. Mostofi, P. D. Haynes, C. J. Pickard, and M. C. Payne, *Comput. Phys. Commun.* **140**, 315 (2001).
- <sup>53</sup>N. D. M. Hine, P. D. Haynes, A. A. Mostofi, C.-K. Skylaris, and M. C. Payne, *Comput. Phys. Commun.* **180**, 1041 (2009).
- <sup>54</sup>L. S. Blackford, J. Choi, A. Cleary, E. D'Azavedo, J. Demmel, I. Dhillon, J. Dongarra, S. Hammarling, G. Henry, A. Petitet, K. Stanley, D. Walker, and R. C. Whaley, *ScaLAPACK Users' Guide* (Society for Industrial and Applied Mathematics, 1997).
- <sup>55</sup>T. Ozaki, *Phys. Rev. B* **64**, 195110 (2001).
- <sup>56</sup>H. Hellmann, *Einführung in die Quantenchemie* (Deuticke, Leipzig, 1937).
- <sup>57</sup>R. P. Feynman, *Phys. Rev.* **56**, 340 (1939).
- <sup>58</sup>N. D. M. Hine, M. Robinson, P. D. Haynes, C.-K. Skylaris, M. C. Payne, and A. A. Mostofi, *Phys. Rev. B* **83**, 195102 (2011).
- <sup>59</sup>P. Pulay, *Mol. Phys.* **17**, 197 (1969).
- <sup>60</sup>A. Ruiz-Serrano, N. D. M. Hine, and C. K. Skylaris, *J. Chem. Phys.* **136**, 234101 (2012).
- <sup>61</sup>M. Weinert and J. W. Davenport, *Phys. Rev. B* **45**, 13709 (1992).
- <sup>62</sup>R. W. Warren and B. I. Dunlap, *Chem. Phys. Lett.* **262**, 384 (1996).
- <sup>63</sup>A. M. N. Niklasson, *J. Chem. Phys.* **129**, 244107 (2008).
- <sup>64</sup>G. P. Kerker, *Phys. Rev. B* **23**, 3082 (1981).
- <sup>65</sup>P. O. Lowdin, *J. Chem. Phys.* **18**, 365 (1950).
- <sup>66</sup>C. K. Gan, P. D. Haynes, and M. C. Payne, *Comput. Phys. Commun.* **134**, 33 (2001).
- <sup>67</sup>C. A. White, P. Maslen, M. S. Lee, and M. Head-Gordon, *Chem. Phys. Lett.* **276**, 133 (1997).
- <sup>68</sup>A. A. Mostofi, P. D. Haynes, C. K. Skylaris, and M. C. Payne, *J. Chem. Phys.* **119**, 8842 (2003).
- <sup>69</sup>A. A. Mostofi, C.-K. Skylaris, P. D. Haynes, and M. C. Payne, *Comput. Phys. Commun.* **147**, 788 (2002).
- <sup>70</sup>J. P. Perdew, K. Burke, and M. Ernzerhof, *Phys. Rev. Lett.* **77**, 3865 (1996).
- <sup>71</sup>B. G. Pfrommer, M. Cote, S. G. Louie, and M. L. Cohen, *J. Comput. Phys.* **131**, 233 (1997).
- <sup>72</sup>L. E. Ratcliff, N. D. M. Hine, and P. D. Haynes, *Phys. Rev. B* **84**, 165131 (2011).
- <sup>73</sup>C.-K. Skylaris and P. D. Haynes, *J. Chem. Phys.* **127**, 164712 (2007).
- <sup>74</sup>B. Hammer, L. B. Hansen, and J. K. Nørskov, *Phys. Rev. B* **59**, 7413 (1999).
- <sup>75</sup>H. J. Monkhorst and J. D. Pack, *Phys. Rev. B* **13**, 5188 (1976).
- <sup>76</sup>F. Birch, *Phys. Rev.* **71**, 809 (1947).